# Scatter correction of 4D cone beam computed tomography to detect dosimetric effects due to anatomical changes in proton therapy for lung cancer

Henning Schmitz, Moritz Rabe, Guillaume Janssens, Simon Rit, Katia Parodi, Claus Belka, Florian Kamp, Guillaume Landry, Christopher Kurz

Received: 24 June 2022 | Revised: 1 February 2023 | Accepted: 14 February 2023

DOI: 10.1002/mp.16335

RESEARCH ARTICLE

MEDICAL PHYSICS

# Scatter correction of 4D cone beam computed tomography to detect dosimetric effects due to anatomical changes in proton therapy for lung cancer

**Henning Schmitz**[1] | **Moritz Rabe**[1] | **Guillaume Janssens**[2] | **Simon Rit**[3] | **Katia Parodi**[4] | **Claus Belka**[1,5] | **Florian Kamp**[1,6] | **Guillaume Landry**[1] | **Christopher Kurz**[1]

[1]Department of Radiation Oncology, University Hospital, LMU Munich, Munich, Bavaria, Germany

[2]Ion Beam Applications SA, Louvain-la-Neuve, Louvain-la-Neuve, Belgium

[3]Univ Lyon, INSA-Lyon, Université Claude Bernard Lyon 1, UJM-Saint Etienne, CNRS, Inserm, CREATIS UMR 5220, U1294, F-69373, Lyon, France

[4]Department of Medical Physics, Ludwig-Maximilians-Universität München (LMU Munich), Garching (Munich), Germany

[5]German Cancer Consortium (DKTK), Partner Site Munich, Munich, Germany

[6]Department of Radiation Oncology, University Hospital Cologne, Cologne, Germany

**Correspondence**
Guillaume Landry.
Email: Guillaume.Landry@med.uni-muenchen.de

Guillaume Landry and Christopher Kurz contributed equally to this study.

**Funding information**
Deutsche Forschungsgemeinschaft, Grant/Award Number: 399148265; Research Training Group GRK, Grant/Award Number: 2274

## Abstract

**Background:** The treatment of moving tumor entities is expected to have superior clinical outcomes, using image-guided adaptive intensity-modulated proton therapy (IMPT).

**Purpose:** For 21 lung cancer patients, IMPT dose calculations were performed on scatter-corrected 4D cone beam CTs ($4DCBCT_{cor}$) to evaluate their potential for triggering treatment adaptation. Additional dose calculations were performed on corresponding planning 4DCTs and day-of-treatment 4D virtual CTs (4DvCTs).

**Methods:** A 4DCBCT correction workflow, previously validated on a phantom, generates 4DvCT (CT-to-CBCT deformable registration) and $4DCBCT_{cor}$ images (projection-based correction using 4DvCT as a prior) with 10 phase bins, using day-of-treatment free-breathing CBCT projections and planning 4DCT images as input. Using a research planning system, robust IMPT plans administering eight fractions of 7.5 Gy were created on a free-breathing planning CT (pCT) contoured by a physician. The internal target volume (ITV) was overridden with muscle tissue. Robustness settings for range and setup uncertainties were 3% and 6 mm, and a Monte Carlo dose engine was used. On every phase of planning 4DCT, day-of-treatment 4DvCT, and $4DCBCT_{cor}$, the dose was recalculated. For evaluation, image analysis as well as dose analysis were performed using mean error (ME) and mean absolute error (MAE) analysis, dose–volume histogram (DVH) parameters, and 2%/2-mm gamma pass rate analysis. Action levels (1.6% ITV D98 and 90% gamma pass rate) based on our previous phantom validation study were set to determine which patients had a loss of dosimetric coverage.

**Results:** Quality enhancements of 4DvCT and $4DCBCT_{cor}$ over 4DCBCT were observed. ITV $D_{98\%}$ and bronchi $D_{2\%}$ had its largest agreement for $4DCBCT_{cor}$–4DvCT, and the largest gamma pass rates (>94%, median 98%) were found for $4DCBCT_{cor}$–4DvCT. Deviations were larger and gamma pass rates were smaller for 4DvCT–4DCT and $4DCBCT_{cor}$–4DCT. For five patients, deviations were larger than the action levels, suggesting substantial anatomical changes between pCT and CBCT projections acquisition.

**Conclusions:** This retrospective study shows the feasibility of daily proton dose calculation on $4DCBCT_{cor}$ for lung tumor patients. The applied method is of clinical interest as it generates up-to-date in-room images, accounting for

breathing motion and anatomical changes. This information could be used to trigger replanning.

**KEYWORDS**
4D, adaptive radiotherapy, CBCT, cone beam CT, lung cancer, proton therapy, scatter correction, virtual CT

## 1 | INTRODUCTION

The favorable ballistics of proton over photon beams allow for substantial dose sparing in organs at risk (OARs), as they deposit considerably less energy in the entrance path, while ensuring target coverage with Bragg peaks.[1] The advancement of pencil-beam intensity-modulated proton therapy (IMPT)[2,3] has led to a better dose conformity than passive beam scattering, which is expected to improve therapeutic results. To fully exploit this potential, the high geometrical selectivity of the beam must be accompanied by imaging allowing to account for inter- and intrafractional changes such as weight loss, tumor shrinkage or growth, and respiratory motion. The superior conformity could thus not only be beneficial for relatively static tumors, like head and neck (H&N) or prostate, but also for moving entities such as lung cancer.

Current clinical practice prioritizes tumor coverage over OAR sparing by applying safety margins around the target. Adaptive radiotherapy (ART) tries to reduce these margins by modifying the treatment plan—if necessary this happens multiple times—in dependence of observed alterations in updated images of patients. These ideally daily images, which are needed for adaptive IMPT,[4,5] could better account for the patient's interfractional changes of respiratory patterns[6] and the subsequent lung tumor motion.[7]

Nevertheless, current image-based corrections in proton therapy are mostly limited to setup uncertainties. Vendors equipped their gantries with cone beam computed tomography (CBCT) scanners,[8] which allow image acquisition in treatment position, and thus 3D anatomy patient alignment.

CBCTs, having artifacts and inaccurate CT numbers, necessitate further image enhancements to be applicable for more sophisticated tasks such as organ delineation or dose calculation. Despite these drawbacks, using already available CBCT scans for dosimetric calculations has the advantage of avoiding additional dose burden for the patient from an additional CT scan. A wide spectrum of CBCT correction methods has been used, including look-up tables[9,10] and Monte Carlo calculations of scatter.[11–13] A promising approach relies on virtual CTs (vCT),[14–16] linking CT and CBCT image pairs through deformable image registration (DIR). Artificial intelligence methods[17,18] have also shown promise and provide clinically acceptable correction times. vCTs may fail for entities with significant interfractional anatomical changes.[19] An alternative is the use of scatter correction algorithms (SCA)[19–24] that utilize the vCT as a prior. Most of these studies focused on 3D images, and the few that considered 4D images typically used a vCT-based approach and focused on phantom validation.[24–26] A 4D scatter correction has, to the best of our knowledge, not yet been applied to lung patient data. This is a challenging problem as data that needs to be binned into the breathing phases very quickly becomes too sparse, which results in poorly reconstructed images.

3D SCA methods, such as those described by Niu et al.[20] and Park et al.,[21] are not directly applicable on 4D data for two reasons: (i) the lower quality of 4D cone beam CT (4DCBCT) reconstruction per breathing phase means that generating a vCT for each phase may be challenging, and (ii) reconstruction of scatter corrected projections with conventional FDK[27] methods may lead to streak artifacts. To address these issues, in this study, we used midposition images for vCT generation, and motion aware reconstruction based on spatial and temporal regularization (MA-ROOSTER).[28] The novelty of this workflow, validated in a ground truth study using a moving porcine lung phantom with programmable breathing motion,[24] is the generation of updated day-of-treatment 4D scatter corrected cone beam images ($4DCBCT_{cor}$) that could be used to trigger offline adaptations.

In this lung patient study, phase-specific dose calculations were performed on $4DCBCT_{cor}$s and compared to corresponding 4DCTs and day-of-treatment 4D virtual CTs (4DvCTs). The scatter correction workflow is applied for the first time for lung patients, which is a necessary and valuable step towards clinical implementation.

## 2 | METHODS

### 2.1 | Patient cohort

Data sets from 21 lung cancer patients treated with photon radiotherapy at the Department of Radiation Oncology at the University Hospital of LMU Munich were employed in this study. For each patient, a free-breathing 4DCT scan with 10 phase bins and a free-breathing 3D planning CT scan (pCT), which was contoured by

**TABLE 1** Patients' characteristics including ITV size and cc motion, number and angles of treatment beams, number of CBCT projections, and time between 4DCT and CBCT projections acquisition $\Delta_t$.

| Patient | Size ITV [$cm^3$] | cc motion [mm] | # Beams | Beam angles [°] | # Projections | $\Delta t$ [d] |
|---|---|---|---|---|---|---|
| 1 | 7.9 | 9 | 3 | 5, 60, 195 | 687 | 6 |
| 2 | 16.3 | 9 | 3 | 10, 170, 280 | 667 | 5 |
| 3 | 298.9 | 12 | 3 | 180, 240, 350 | 690 | 8 |
| 4 | 228.5 | 9 | 3 | 0, 180, 210 | 665 | 12 |
| 5 | 2.4 | 10 | 3 | 220, 270, 350 | 672 | 14 |
| 6 | 17.6 | 6 | 3 | 0, 160, 200 | 682 | 9 |
| 7 | 3.4 | 6 | 3 | 0, 180, 280 | 678 | 12 |
| 8 | 35.0 | 15 | 3 | 0, 90, 180 | 701 | 15 |
| 9 | 23.2 | 6 | 3 | 20, 90, 150 | 681 | 7 |
| 10 | 14.0 | 6 | 3 | 5, 60, 220 | 675 | 13 |
| 11 | 2.1 | 6 | 3 | 0, 180, 270 | 658 | 10 |
| 12 | 14.0 | 6 | 3 | 0, 180, 245 | 647 | 11 |
| 13 | 26.5 | 9 | 2 | 155, 210 | 654 | 14 |
| 14 | 20.4 | 6 | 2 | 80, 175 | 681 | 20 |
| 15 | 64.9 | 12 | 3 | 0, 160, 270 | 663 | 16 |
| 16 | 17.1 | 6 | 3 | 0, 70, 190 | 695 | 9 |
| 17 | 1.1 | 6 | 3 | 0, 180, 230 | 685 | 11 |
| 18 | 8.0 | 12 | 3 | 180, 230, 270 | 675 | 11 |
| 19 | 92.7 | 21 | 3 | 80, 150, 190 | 662 | 14 |
| 20 | 7.5 | 6 | 3 | 25, 150, 200 | 663 | 8 |
| 21 | 62.7 | 8 | 3 | 15, 80, 160 | 682 | 10 |
| Median | 17.1 | 8 | 3 | | 675 | 11 |

a trained radiation oncologist, as well as corresponding measured CBCT projections of one arbitrary treatment fraction were used. The 4DCT and the pCT were acquired sequentially at the same appointment. As several acquisition protocols are used clinically, we focused on CBCT scans with more than 600 projections (projections per patient are listed in Table 1). Additionally, the tumor motions on the 4DCT scans were required to be at least 6 mm in cranial-caudal (cc) direction. The onboard CBCT imaging system of an Elekta Synergy or VersaHD linac (XVI 4.5.1, Elekta, Sweden) was used for CBCT acquisitions with a shifted detector (collimator = M20, M position, tube current = 40 mA, tube voltage = 120 kVp, exposure time = 40 ms). A Toshiba Aquilion LB (Canon Medical Systems, Japan) CT scanner was used to acquire pCTs and 4DCTs with a reconstruction grid of $1.074 \times 1.074 \times 3\,\text{mm}^3$.

## 2.2 | 4DCBCT$_{cor}$ workflow

For this study we decided to use a scatter correction workflow based on projection data.[19–22,24] In a 4D scenario, a 4DvCT is needed as a prior. CT to CBCT deformation from phase to phase for a moving entity, such as the lung, is a challenging task due to CBCT undersampling, which may lead to poor results. To address this, we used the midposition approach,[29] generating motion-reduced average images, which benefit from full sampling. To further mitigate motion artifacts MAROOSTER, an iterative reconstruction algorithm, which combines motion-estimation and motion-compensated reconstruction methods with regularized 4D reconstruction methods,[28] was used.

A sketch of the workflow up to the dose calculation is shown in Figure 1. The inputs, that is, the initial planning 4DCT and the day-of-treatment CBCT projections, are shown in blue. Out of those inputs an average CT, generated from the 4DCT, and a 3DCBCT (FDK[27] reconstruction) were rigidly registered using Mattes Mutual information with 6 degrees of freedom. This registration was not sufficient for a few patients and thus an additional registration step was performed. A box was drawn manually at a static body region such as the spine so that an additional rigid registration could focus on that region. Successively, a composition of the transformation matrices from both registrations was used to move the 4DCT to the CBCT space. The pCT and the corresponding structures, which are not used specifically within the 4DCBCT$_{cor}$ workflow, were also moved with the same registration to the CBCT space so that all images were on the same grid for the proton dose

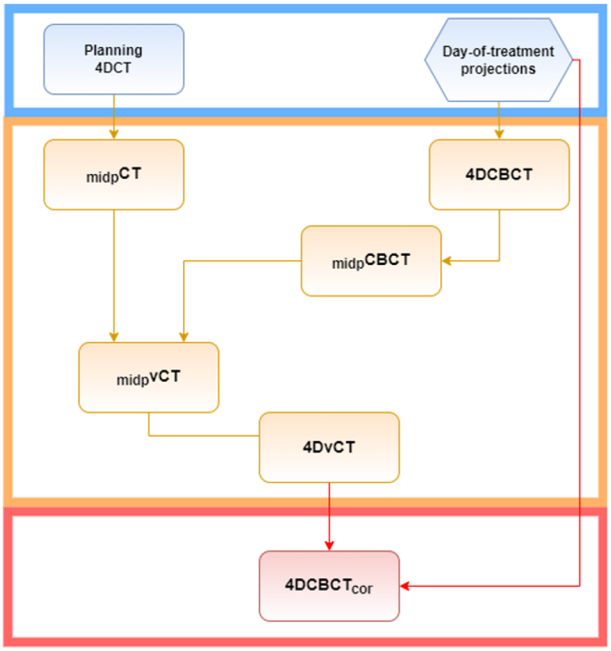


**FIGURE 1** Sketch depicting the different images and data used and generated within the 4DCBCT scatter correction workflow. The input is shown in blue. The orange box represents the 4DvCT generation, and the red box shows the scatter correction. 4DCBCT, 4D cone beam CT; 4DvCT, 4D virtual CT.

planning (using an average CT calculated from the 4DCT, cf. Section 2.3).

The orange box represents the 4DvCT generation. The Amsterdam Shroud algorithm[30] applies a superior–inferior derivative to enhance features in the dominant breathing direction. The concatenation of transversely summed pixels of all individual projections yields the Amsterdam Shroud image, which shows the oscillatory signal. This signal was used to split the CBCT projection data into 10 phases. Successively, the following steps are done to generate a midposition CT (midpCT) from the 4DCT: all phases are registered to a reference phase, for which we chose the maximum expiration phase due to the high reproducibility, yielding deformable vector fields (DVFs). The inverse of the mean motion vector, which is the average of all DVFs, is composed with each of the original DVFs, yielding new DVFs. Applying these new DVFs to their corresponding phase of the 4DCT and taking the median of the generated set of deformed 4DCT phases yields the midposition image. Using the DVFs from this midposition process, the 4DCBCT was reconstructed using MA-ROOSTER,[28] which is implemented in RTK.[31] Diffeomorphic Morphons,[32] which instead of using pixel intensities matches intensity gradients, was used for the multimodal registration of midposition images of the 4DCT ($_{midp}$CT) to midposition images of the 4DCBCT ($_{midp}$CBCT), yielding the midposition virtual CT ($_{midp}$vCT). The inverted deformable vector fields (DVF) of the 4DCBCT mid-position generation were applied subsequently to the $_{midp}$vCT to obtain the moving 4DvCT. The 4DvCT generation was implemented in OpenREGGUI (https://openreggui.org/). The red box displays the per-phase 4DCBCT SCA. The projection error, which is the difference of the forward projected vCT and the measured projections plus a generous smoothing filter (see Kurz et al.[19] for exact details), is subtracted from the measured projections yielding corrected projections. With these corrected projections, the 4DCBCT$_{cor}$ was reconstructed applying the same settings used for the 4DCBCT reconstruction.

With the isocenter located at the tumor, the CBCT field of view (FOV) did not always cover the contralateral lung. Therefore, before input to the SCA, the 4DvCT was stitched using the 4DCT outside of the CBCT FOV to provide correct forward projections. For the vCT, all values outside and for the CT all values inside the CBCT FOV were set to zero. The sum of these modified vCT and CT images, yielded the stitched vCT. Figure A.1 in the appendix shows the individual images for patient 14.

A comprehensive description of the workflow is outlined in the previous phantom-based validation study[24] (except for stitching, which was not needed in that previous study).

## 2.3 | Treatment planning

All 10 phases of 4DCT, 4DvCT, and 4DCBCT$_{cor}$ as well as the pCT, using the same generic CT number to density calibration curve, were transferred to the research version 10.1.100.0 of the commercial treatment planning system RayStation (RaySearch Laboratories, Sweden). We used a beam model ("RSL_PBS_CYC") corresponding to a generic pencil beam scanning beamline and nozzle (available energy range: 70–230 MeV; nominal spot size (1$\sigma$) at isocenter: 7.0 mm (70 MeV)/2.7 mm (230 MeV); Bragg peak width at 80% dose level: 1.7 mm (70 MeV)/8.5 mm (230 MeV); hexagonal spot scanning pattern with automatic spot spacing of 1.06 times 1$\sigma$ of the lateral Bragg peak spread; automatic energy layer spacing corresponding to the width at 80% dose level of the more distant Bragg peak. All outer contours were created using a threshold of −500 HU and manually adapted if it was considered necessary.

A density override of the internal target volume (ITV), which is the union of the gross target volumes (GTV) delineation on each phase of the 4DCT, was performed on the pCT using muscle tissue with a density of 1.05 g cm$^{-3}$.[33,34]

Robustly optimized 3D pencil beam scanning IMPT plans, administering 60 Gy in eight fractions, were created on the pCTs. A range shifter of 7.5 cm was added to each plan. The beams were optimized individually, resulting in SFUD plans.

The ITV among the investigated patients had a volume ranging from 1.1 to 298.9 cm$^3$ with a median

**TABLE 2** Summarized results from the phantom study.[24]

| | vCT-CT | CBCTcor-CT | Action levels |
|---|---|---|---|
| ITV D98% | 0.9% [0.1%, 1.3%] | 1.2% [0.8%, 1.6%] | 1.6% |
| Gamma PR (2%, 2 mm) | 94.7% [93.2%, 97.5%] | 95.8% [94.2%, 97.9%] | 90% |

The values shown are median, minimum, and maximum of the target dose expressed in the DVH parameter ITV $D_{98\%}$ and the gamma PR, which covers the dose volume covered by 10% isodose. The third column shows the selected action levels used for the proton dose analysis of the lung patients.

value of 17.1 $cm^3$. Its motion in cc direction ranged from 6 to 21 mm with a median value of 8 mm. Additional patient specific information, which is relevant for the planning process (ITV volume, ITV motion, number of beams, and beam angles), can be found in Table 1.

A Monte Carlo dose engine with a statistical error of 1% during plan optimization was used. Each plan assumed a constant relative biological effectiveness (RBE) of 1.1.[35] Clinical robustness settings were 3% range and 6-mm setup uncertainty,[33] which led to a total number of scenarios or optimization dose computations of 45 (3 range scenarios times 15 setup scenarios). Following Fredriksson et al.,[36] the robust optimization used a minimax method, considering the worst-case scenario with regards to the optimization functions. The objectives for the ITV were a minimum dose of 60 Gy, a maximum dose of 70 Gy, and a uniform dose of 60 Gy. The objectives for the considered OARs esophagus, heart, and bronchi were a maximum dose of 43, 65, and 46 Gy, respectively.

Subsequently, the dose was recomputed without density override on all 10 phases of the different modalities (planning 4DCT, day-of-treatment 4DvCT, and 4DCBCT$_{cor}$).

## 2.4 | Data analysis

A comparison between the different modalities was conducted by analyzing difference images as well as mean error (ME) and mean absolute error (MAE) plots. For ME and MAE, the investigated contour was the union of the CBCT FOV with the CT body outline. In the following, when discussing phases of the 4DCT, 4DCBCT, 4DvCT, and 4DCBCT$_{cor}$, we will use CT, CBCT, vCT, and CBCT$_{cor}$ and omit the 4D prefix. CT should not be confused with pCT. Proton doses were calculated (interplay effects were not considered and the full plan was calculated on each phase), so that a pairwise comparison of the dose calculated on generated images to the dose calculated on the CT (difference vCT–CT and CBCT$_{cor}$–CT) as well as among the generated images (difference CBCT$_{cor}$–vCT) could be determined for each phase. Further evaluation of the corresponding dose values was done by comparing dose–volume histogram (DVH) parameters (bronchi $D_{2\%}$, ITV $D_{98\%}$, lung $D_{mean}$) and calculating global gamma pass-rates (PR) using a (2%, 2 mm) criterion with a fixed dose threshold of 10% of the prescribed dose. The necessary structure delineations were rigidly copied from the pCT. The results are compared to those, obtained in a phantom study, which are listed in Table 2. That study had a ground truth 4DCT image with the same anatomy and breathing pattern as the 4DCBCT, using a porcine lung phantom.[24] This let us calculate the expected accuracy of the method, and set thresholds where greater differences can be considered clinically relevant and detectable by our methodology.

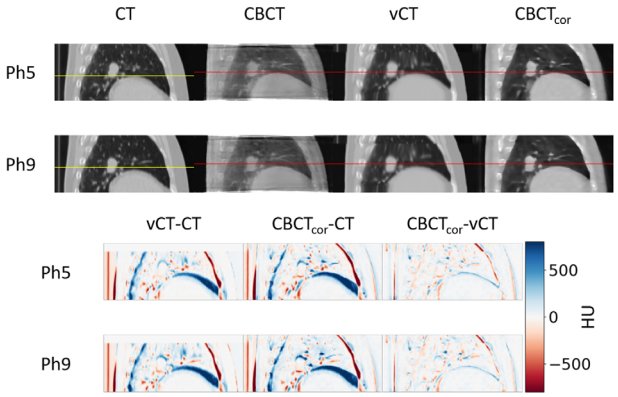


**FIGURE 2** Exhale (ph5) and inhale (ph9) phases of patient 14 for CT, CBCT, vCT, and CBCT$_{cor}$ are displayed using window = 1600 and level = −300 in the top two rows. The horizontal lines indicate the exhale diaphragm position (yellow ≙ CT and red ≙ CBCT). Difference images of vCT–CT, CBCT$_{cor}$–CT, and CBCT$_{cor}$–vCT showing deviations in Hounsfield units are shown in the bottom two rows. The stitching of the vCT (top part in this view) is by definition the CT and thus their difference in this area is 0. CBCT, cone beam computed tomography; vCT, virtual CT.

# 3 | RESULTS

## 3.1 | Comparison between different modalities

Figure 2 displays a fixed sagittal slice of CT, CBCT, vCT, and CBCT$_{cor}$ for phases 5 (exhale) and 9 (inhale) as well as corresponding image differences of patient 14. vCT and CBCT$_{cor}$ show improved image quality compared to the CBCT. The structures in the lung in the CBCT$_{cor}$ appear less distorted than in the vCT. At the diaphragm–lung interface in the difference images vCT–CT and CBCT$_{cor}$–CT, differences of more than 500 HU were observed. In comparison, the differences between

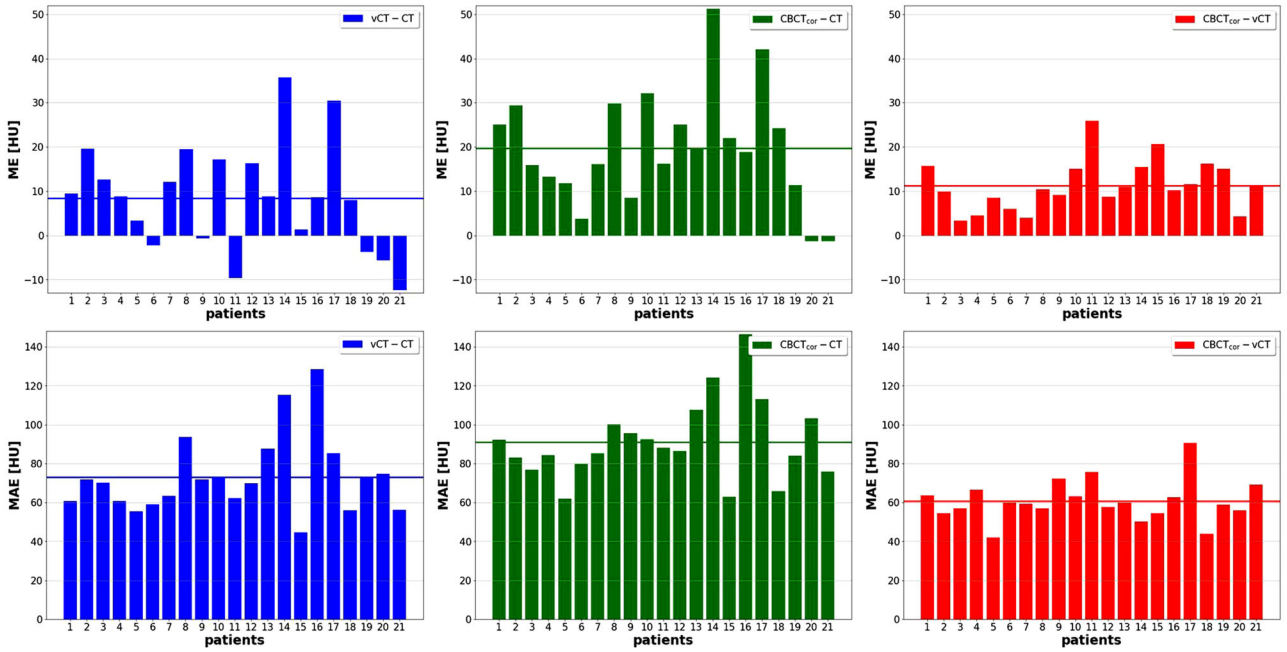


**FIGURE 3** ME and MAE plots for the comparisons vCT–CT, CBCT$_{cor}$–CT, and CBCT$_{cor}$–vCT for all patients averaged over the 10 breathing phases. Horizontal lines show the mean value over all patients. CBCT, cone beam computed tomography; MAE, mean absolute error; ME, mean error; vCT, virtual CT.

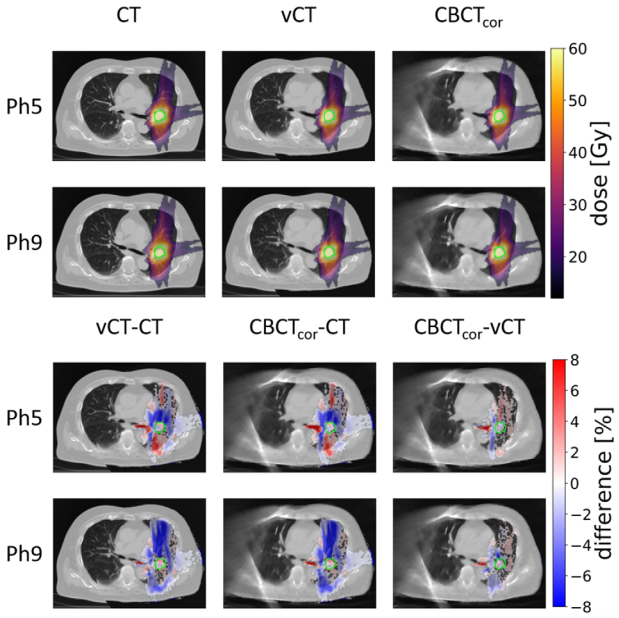


**FIGURE 4** Recalculated proton dose distributions and their differences on the three considered images for patient 14. This patient shows large differences. For better readability of the difference plots (expressed as a percentage of the prescribed dose), dose difference values smaller than 0.4% are masked. Areas outside the CBCT FOV in the vCT are stitched with the planning CT. CBCT, cone beam computed tomography; FOV, field of view; vCT, virtual CT.

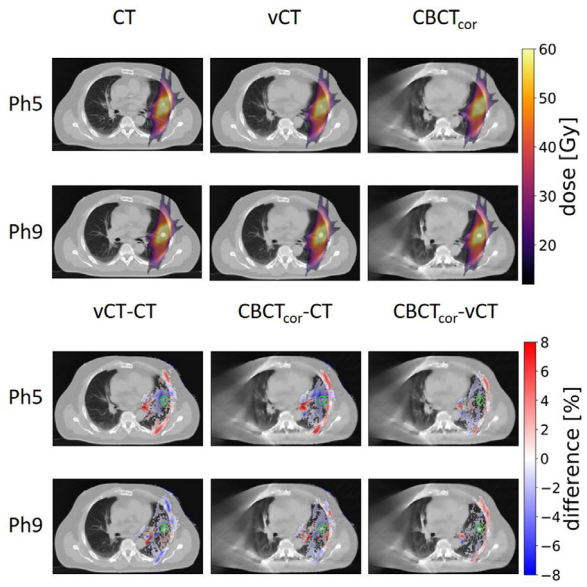


**FIGURE 5** Recalculated proton dose distributions and their differences analogous as in Figure 4 for patient 1. This patient shows small differences.

CBCT$_{cor}$ and vCT were small. The stitching is visible in the top part of the vCT. Consequently, the same part in the difference image vCT–CT is by definition 0.

Figure 3 shows for the three different comparisons vCT–CT, CBCT$_{cor}$–CT, and CBCT$_{cor}$–vCT a ME and MAE analysis. The displayed data are averaged over the 10 breathing phases for each patient. Average values for the comparisons over all patients are 8.4, 19.7, and 11.3 HU for ME and 73.0, 91.0, and 60.7 HU for MAE.

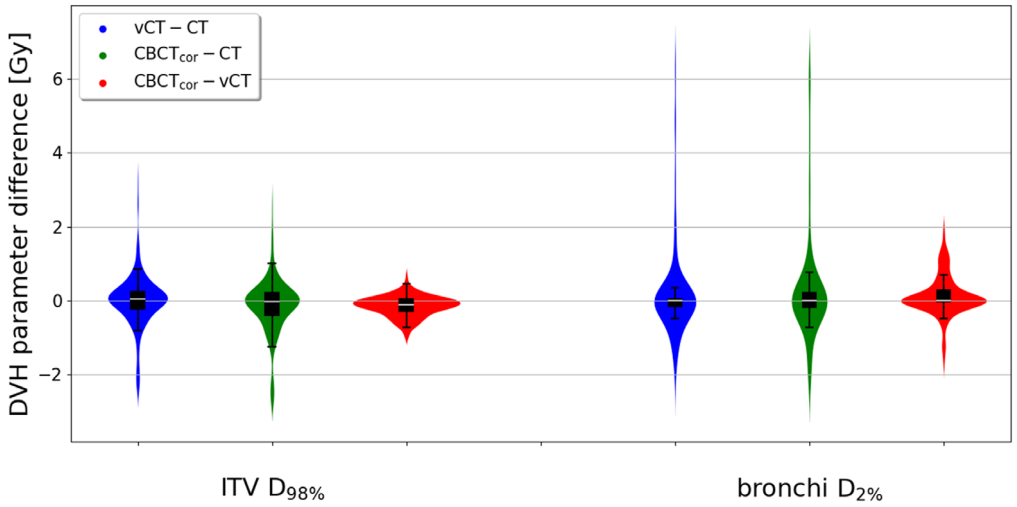


**FIGURE 6** Violin plots showing the DVH parameter differences of all phases of all 21 patients for ITV $D_{98\%}$ and bronchi $D_{2\%}$ for vCT–CT, $CBCT_{cor}$–CT, and $CBCT_{cor}$–vCT. Additionally, box plots with the median value shown as a white horizontal line and a whisker length of 1.5 times the interquartile range (range from Q1 to Q3 ≙ length of the box) are displayed. Outliers are not shown for the box plots. CBCT, cone beam computed tomography; DVH, dose–volume histogram; ITV, internal target volume; vCT, virtual CT.

## 3.2 | Proton dose analysis

Figure 4 displays an axial slice for phases 5 (exhale) and 9 (inhale) of proton dose distributions calculated on the individual phases of patient 14 for CT, vCT, and $CBCT_{cor}$, and their respective dose differences. Patient 14 was selected since we suspect anatomical differences based on gamma PR analysis (results in Table 2) between 4DCT and 4DCBCT. The dose difference plots show minor deviations of less than 4% between $CBCT_{cor}$ and vCT with the exception of the bronchi area. Larger differences of more than 8% are observed for the differences vCT–CT and $CBCT_{cor}$–CT. Note that we did not use stitching for $CBCT_{cor}$ in the contralateral lung where dose calculation is not necessary. Figure 5 shows a similar plot for patient 1 with substantially smaller deviations for the calculated doses. For patient 1, gamma PR analysis does not suggest anatomical changes between 4DCT and 4DCBCT. The time between 4DCT and CBCT projections acquisition $\Delta t$ is with 20 days the largest for patient 14 (cf. Table 1). Patient 1 has the second smallest $\Delta t$ with 6 days.

Figure 6 displays DVH parameter differences of vCT–CT, $CBCT_{cor}$–CT, and $CBCT_{cor}$–vCT for ITV $D_{98\%}$ and bronchi $D_{2\%}$ of all patients in a violin and box plot. Regarding the different distributions, the highest similarity for each DVH parameter is observed between $CBCT_{cor}$ and vCT. Overall, the medians of the differences are centered around zero. Additionally, the mean lung dose was similar with median dose difference below 0.1 Gy.

Absolute dose values of ITV $D_{98\%}$, showing that the dose target for the plan of 60 Gy is mostly met for the recalculation on the individual phases, are shown in Figure A.2 in the appendix.

Figure 7 displays for all patients differences in the DVH parameter ITV $D_{98\%}$. For most of the patients and comparisons, the differences are small as they are centered around 0. To compare the results with our previous phantom study, horizontal lines at $\pm 1.6\% \cdot 60$ Gy, which is the largest observed deviation in the phantom case, are drawn (cf. Table 2). Patients 3, 8, 9, 16, 19, and 21 show larger difference for the comparisons of vCT–CT and $CBCT_{cor}$–CT than the maximum deviation detected in the phantom study. The comparison $CBCT_{cor}$–vCT never exceeds this threshold.

Figure 8 shows a similar plot for the OAR DVH parameter bronchi $D_{2\%}$. Patients without a contoured bronchi structure are not shown. A direct comparison to the phantom results is not possible as the phantom did not have bronchi segmentations.

Table 3 summarizes the quantitative results of the proton dose comparison displaying median, minimum, and maximum gamma PR for a (2%/2 mm) criterion for each patient. For all patients, the median of $CBCT_{cor}$–vCT is larger than the median of either vCT–CT or $CBCT_{cor}$–CT, which can also be seen in the median values of all patients, which are 98, 92, and 91%, respectively.

The lowest PR are found for patients 8 and 14 for the comparisons of vCT–CT and $CBCT_{cor}$–CT with minimum values of 75 and 74%, while the median values of the same patients for the comparison $CBCT_{cor}$–vCT are 99 and 98%. Values below 90% occurred for patients 3, 6, 7, 8, 9, 13, 14, 16, and 21. The threshold of 90%, which is close to the smallest value of 93.2% observed in the phantom study (cf. Table 2), is used to highlight larger deviations.

The largest agreement is observed for patient 1 with median values of 98, 97, and 100% for vCT–CT, $CBCT_{cor}$–CT, and $CBCT_{cor}$–vCT, respectively.

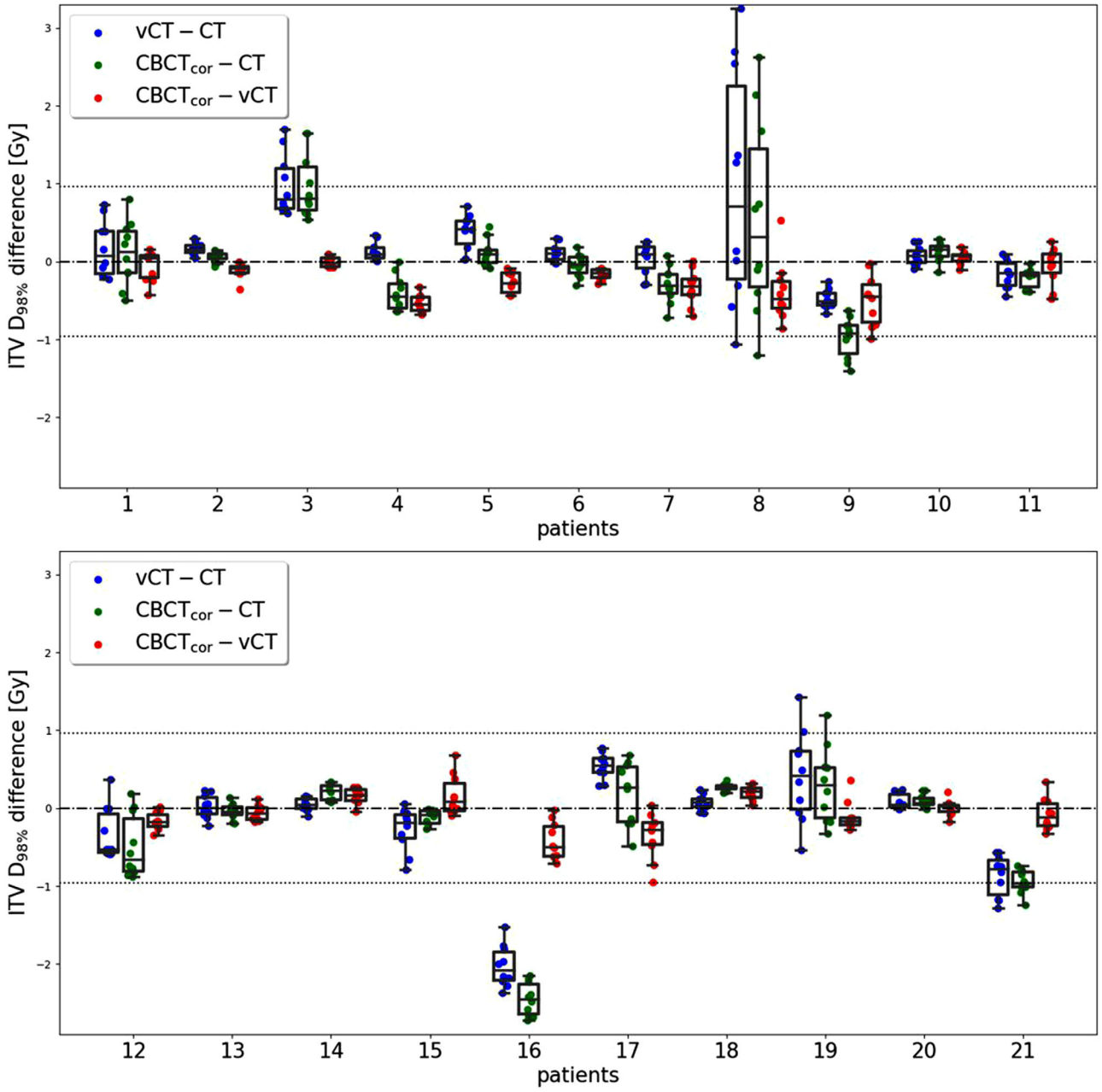


**FIGURE 7** The differences in ITV $D_{98\%}$ of all breathing phases (individual data-points) of all 21 patients for vCT-CT, $CBCT_{cor}$-CT, and $CBCT_{cor}$-vCT are shown as box plots. The box plots display the median value as a black horizontal line and have a whisker length of 1.5 times the interquartile range (range from Q1 to Q3 ≙ length of the box). Horizontal lines are drawn at $\pm 1.6\% \cdot 60$ Gy to compare the results to those obtained in the ground truth study, using a porcine lung phantom. CBCT, cone beam computed tomography; ITV, internal target volume; vCT, virtual CT.

## 4 | DISCUSSION

This work presents the first retrospective application of a previously phantom-validated[24] 4DCBCT scatter correction approach to a clinically treated lung cancer cohort. For 21 patients, IMPT plans were created. A comprehensive dosimetric analysis that compared CT, vCT, and $CBCT_{cor}$ showed that the largest agreements were found between vCT and $CBCT_{cor}$. After the proof-of-concept study with the phantom, the presented study is the next step towards a potential clinical application in the evaluation of this method.

The investigated tumor sizes ranged from 1.1 to 298.9 $cm^3$, which is in accordance to reported volumes from 4 to 776 $cm^3$ in a nonsmall-cell lung cancer study that analyzed volume changes.[37] A study by Wolthaus et al.[38] investigated a lung cohort with motion in cc ranging from 0.8 to 24 mm, which shows that our cohort has a focus on slightly larger motion as the smallest value was 6 mm and the largest was 21 mm. The same

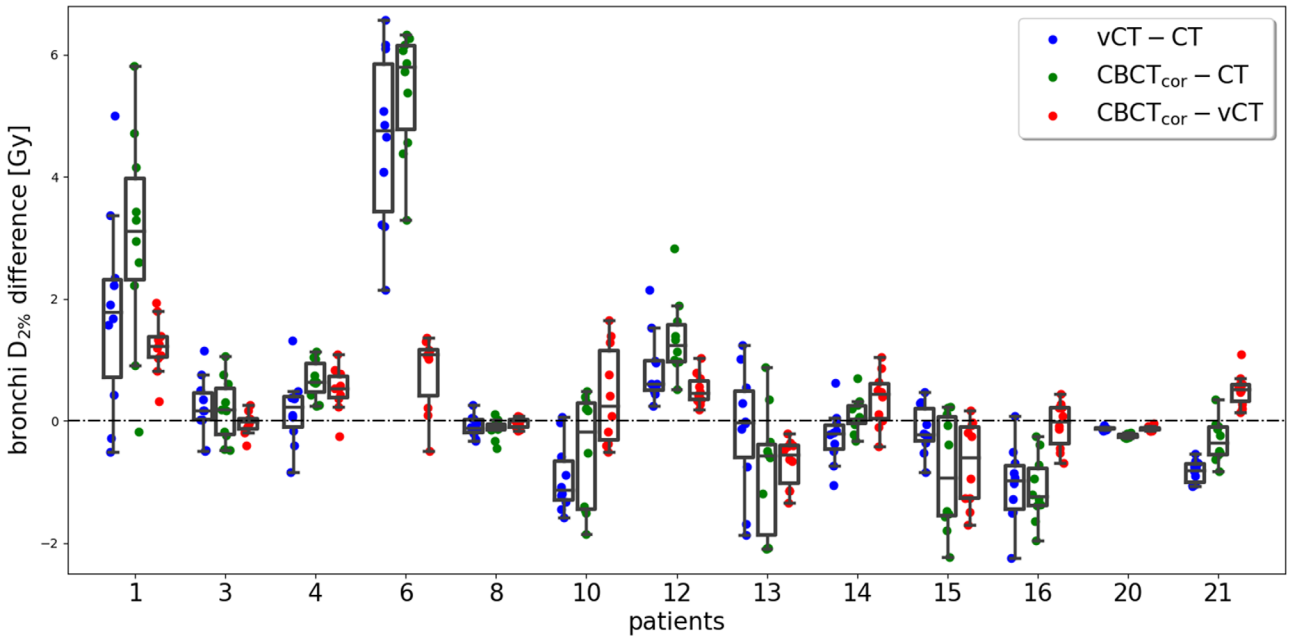


**FIGURE 8** Differences in the DVH parameter bronchi $D_{2\%}$ are shown for the comparisons vCT-CT, $CBCT_{cor}$-CT, and $CBCT_{cor}$-vCT. Patients without a contoured bronchi structure are omitted. The box plots show the median values as a black horizontal line and have a whisker length of 1.5 times the interquartile range. CBCT, cone beam computed tomography; DVH, dose–volume histogram; vCT, virtual CT.

study presented GTV volumes from 2 to 200 $cm^3$, which again indicates that the tumors for our patients were distributed within a normal clinical range.

The qualitative image analysis showed that vCT and $CBCT_{cor}$ are superior in image quality compared to the day-of-treatment CBCT,[19,21] and additionally display correctly the patient's breathing motion. This is especially noticeable in the difference images (Figure 2) at the lung–diaphragm interface, where large baseline shifts occur between the vCT–CT and $CBCT_{cor}$–CT. Regarding the tumor outline and ribs, higher geometric fidelity of the $CBCT_{cor}$ over the vCT and thus better image adaptation to the patients' anatomical changes could be observed, which is in accordance to previous studies.[19]

Planning was conducted on 3D CT images with a total dose of 60 Gy prescribed to the ITV. The recalculation of these plans on individual phases was robust, which can be seen in Figure A.2 in the appendix, as median values of ITV $D_{98\%}$ for CT, vCT, and $CBCT_{cor}$ are slightly above 59 Gy. We observed that to achieve this with our current robustness settings, it was necessary to optimize the beams independently. Doses for OARs achieved their target constraints as medium values for, for example, bronchi $D_{2\%}$ were below 10 Gy for CT, vCT, and $CBCT_{cor}$.

Larger dose differences for vCT–CT and $CBCT_{cor}$–CT than for $CBCT_{cor}$–vCT indicate anatomical or breathing changes, which are accounted for in the vCT and $CBCT_{cor}$ as they show the same day-of-treatment anatomy and breathing motion as the CBCT. Consequently, those images then differ to the pCT. Differences of vCT and $CBCT_{cor}$ to the CT have the same tendencies, which again hints to the aforementioned changes and an absence of stochastic errors.

Similar conclusions can be drawn regarding the dose difference shown in the violin and box plots in Figure 6. The distribution for the comparison of $CBCT_{cor}$ and vCT is narrower around 0 for both ITV $D_{98\%}$ and bronchi $D_{2\%}$ than in the two other cases. Comparing doses at an individual level (per patient), dose differences among the 10 phases validate the statement of a clear tendency of differences for vCT–CT and $CBCT_{cor}$–CT.

The median gamma PR of vCT–CT and $CBCT_{cor}$–CT are 92 and 91% and thus considerably lower than that of $CBCT_{cor}$–vCT with 98%. This is comparable to previous studies, which also showed high similarity between $CBCT_{cor}$ and vCT.[19] This again indicates that the vCT and $CBCT_{cor}$ account for anatomical or breathing pattern changes consistently. However, for patients 1, 2, 5, 10, 15, and 18, all median values of all corresponding images are within less than 3%, which suggests that limited changes took place between the planning and fraction days.

A potential indicator for the necessity of replanning could be large differences in target coverage compared to those observed in the ground truth phantom study. The phantom study could show that the generated 4DvCT and $4DCBCT_{cor}$ were accurate as their image and dose differences to a 4DCT ground truth image with the same anatomy and breathing pattern as the 4DCBCT were small. Consequently, large differences, which occurred for patients 3, 8, 9, 16, 19, and 21, most likely indicate breathing pattern or anatomical changes. Considering gamma PR values below 90%, being less

**TABLE 3** Gamma-index PR in percent for a global criterion of 2%/2 mm with a fixed dose threshold of 10% of the prescribed dose for all patients individually.

| Patient | vCT-CT Median [min, max] | $CBCT_{cor}$-CT Median [min, max] | $CBCT_{cor}$-vCT Median [min, max] |
|---|---|---|---|
| 1 | 98 [97, 99] | 97 [95, 98] | 100 [99, 100] |
| 2 | 97 [96, 98] | 97 [97, 97] | 99 [99, 100] |
| 3 | **81 [80, 83]** | **82 [81, 84]** | 97 [95, 99] |
| 4 | 91 [87, 91] | 91 [89, 92] | 94 [91, 97] |
| 5 | 96 [93, 99] | 95 [90, 97] | 97 [95, 98] |
| 6 | 93 [90, 94] | **88 [85, 91]** | 98 [96, 99] |
| 7 | **88 [84, 92]** | 91 [89, 93] | 97 [96, 97] |
| 8 | **87 [75, 96]** | **86 [78, 93]** | 99 [92, 100] |
| 9 | **78 [76, 83]** | **77 [73, 84]** | 98 [98, 99] |
| 10 | 96 [91, 97] | 97 [94, 98] | 99 [98, 100] |
| 11 | 90 [84, 94] | 94 [89, 96] | 96 [93, 99] |
| 12 | 93 [84, 97] | 91 [82, 95] | 99 [98, 99] |
| 13 | **86 [84, 94]** | **87 [83, 94]** | 96 [94, 98] |
| 14 | **80 [75, 83]** | **79 [74, 81]** | 98 [98, 99] |
| 15 | 97 [96, 98] | 97 [96, 98] | 98 [95, 99] |
| 16 | **85 [83, 87]** | **83 [81, 85]** | 99 [99, 99] |
| 17 | 92 [90, 94] | 93 [92, 96] | 97 [95, 97] |
| 18 | 96 [91, 99] | 97 [92, 99] | 98 [97, 99] |
| 19 | 97 [93, 98] | 95 [93, 98] | 99 [96, 100] |
| 20 | 93 [90, 95] | 91 [89, 93] | 99 [99, 100] |
| 21 | **89 [88, 95]** | **87 [86, 94]** | 99 [99, 99] |
| median | 92 [88, 95] | 91 [89, 94] | 98 [96, 99] |

Values below 90%, being less than the smallest observed value in the phantom study, are in bold.

than the smallest value observed for the phantom study, could be an additional indicator with respect to replanning. Those were observed for patients 3, 6, 7, 8, 9, 13, 14, 16, and 21, respectively. The intersection of these two sets, being patients 3, 8, 9, 16, and 21, could consequently be suggested for replanning.

The overall PR values are in the same range presented by a lung study of Thing et al.,[39] showing results of 93.1 and 99.4% for a clinically used corrected CBCT, and an improved corrected CBCT each compared to a replanning CT. It should be noted that better agreements in their 3D study are expected as motion effects are averaged out and due to the fact that they are comparing their generated images to a replanning CT, which has almost the same anatomy.

A ground truth analysis of vCT and $CBCT_{cor}$ is not possible due to unavoidable breathing pattern changes between image acquisitions, yet we are confident regarding their accuracy due to our phantom validation.

Our method could potentially be limited to large volume changes in the lung. These changes could lead to wrong deformations and thus necessitate post processing of the 4DvCT to fill or empty cavities.[14] This situation did not occur within our current data cohort.

The computation time, which is not optimized, of roughly 4 h per patient is an issue that needs to be addressed for clinical online application. Artificial intelligence approaches for 4DCBCTs may solve this issue[40] and the $4DCBCT_{cor}$ images could be used for paired training of an AI solution similarly to works by Hansen et al. and Landry et al.[41,42]

## 5 | CONCLUSION

In this retrospective study, a previously phantom-validated $4DCBCT_{cor}$ method, based on a phase-per-phase scatter correction using 4DvCT as a prior, has been investigated for proton dose calculations of 21 lung cancer patients. Deviations in proton dose distributions from 4DCT can be observed in both 4DvCT and $4DCBCT_{cor}$. Accounting for anatomical changes and breathing motion, the employed method generated daily in-room images, which could be used for indicating the necessity of plan adaptation and thus are of clinical interest.

## ACKNOWLEDGMENTS

Roel Shpani and Jan Hofmaier are thanked for their support related to treatment planning. Additionally, Martin Hillbrand is thanked for his valuable insights into proton planning. This work was supported by the German Research Foundation (DFG) project number 399148265 and Research Training Group GRK 2274.

Open access funding enabled and organized by Projekt DEAL.

## CONFLICT OF INTEREST STATEMENT

The authors declare no conflicts of interest.

## REFERENCES

1. Berman A, James S, Rengan R. Proton beam therapy for non-small cell lung cancer: current clinical evidence and future directions. *Cancers*. 2015;7:1178-1190.
2. Lomax AJ, Boehringer T, Coray A, et al. Intensity modulated proton therapy: a clinical example. *Med Phys*. 2001;28:317-324.
3. Lomax AJ, Pedroni E, Rutz HP, Goitein G. The clinical potential of intensity modulated proton therapy. *Z Med Phys*. 2004;14:147-152.
4. Hoffmann L, Alber M, Jensen MF, Holt MI, Møller DS. Adaptation is mandatory for intensity modulated proton therapy of advanced lung cancer to ensure target coverage. *Radiother Oncol*. 2017;122:400-405.
5. Villarroel EB, Geets X, Sterpin E. Online adaptive dose restoration in intensity modulated proton therapy of lung cancer to account for inter-fractional density changes. *Phys Imaging Radiat Oncol*. 2020;15:30-37.
6. McClelland JR, Hughes S, Modat M, et al. Inter-fraction variations in respiratory motion models. *Phys Med Biol*. 2010;56:251-272.
7. Knybel L, Cvek J, Molenda L, Stieberova N, Feltl D. Analysis of lung tumor motion in a large sample: patterns and factors

influencing precise delineation of internal target volume. *Int J Radiat Oncol Biol Phys*. 2016;96:751-758.
8. Landry G, ho Hua C. Current state and future applications of radiological image guidance for particle therapy. *Med Phys*. 2018;45:e1086-e1095.
9. Fotina I, Hopfgartner J, Stock M, Steininger T, Lütgendorf-Caucig C, Georg D. Feasibility of CBCT-based dose calculation: comparative analysis of HU adjustment techniques. *Radiother Oncol*. 2012;104:249-256.
10. Kurz C, Dedes G, Resch A, et al. Comparing cone-beam CT intensity correction methods for dose recalculation in adaptive intensity-modulated photon and proton therapy for head and neck cancer. *Acta Oncol*. 2015;54:1651-1657.
11. Mainegra-Hing E, Kawrakow I. Variance reduction techniques for fast Monte Carlo CBCT scatter correction calculations. *Phys Med Biol*. 2010;55:4495-4507.
12. Thing RS, Bernchou U, Mainegra-Hing E, Hansen O, Brink C. Hounsfield unit recovery in clinical cone beam CT images of the thorax acquired for image guided radiation therapy. *Phys Med Biol*. 2016;61:5781-5802.
13. Zöllner C, Rit S, Kurz C, et al. Decomposing a prior-CT-based cone-beam CT projection correction algorithm into scatter and beam hardening components. *Phys Imaging Radiat Oncol*. 2017;3:49-52.
14. Veiga C, Janssens G, Teng C-L, et al. First clinical investigation of cone beam computed tomography and deformable registration for adaptive proton therapy for lung cancer. *Int J Radiat Oncol Biol Phys*. 2016;95:549-559.
15. Veiga C, Janssens G, Baudier T, et al. A comprehensive evaluation of the accuracy of CBCT and deformable registration based dose calculation in lung proton therapy. *Biomed Phys Eng Express*. 2017;3:015003.
16. Cole AJ, Veiga C, Johnson U, D'Souza D, Lalli NK, McClelland JR. Toward adaptive radiotherapy for lung patients: feasibility study on deforming planning CT to CBCT to assess the impact of anatomical changes on dosimetry. *Phys Med Biol*. 2018;63:155014.
17. Thummerer A, Zaffino P, Meijers A, et al. Comparison of CBCT based synthetic CT methods suitable for proton dose calculations in adaptive proton therapy. *Phys Med Biol*. 2020;65:095002.
18. Qin A, Chen S, Liu G, et al. The feasibility and accuracy of utilizing CBCT and generative-adversarial-network (GAN) to perform proton treatment dose evaluation for lung and head and neck patients. *Int J Radiat Oncol Biol Phys*. 2020;108:S41-S42.
19. Kurz C, Kamp F, Park Y-K, et al. Investigating deformable image registration and scatter correction for CBCT-based dose calculation in adaptive IMPT. *Med Phys*. 2016;43:5635-5646.
20. Niu T, Sun M, Star-Lack J, Gao H, Fan Q, Zhu L. Shading correction for on-board cone-beam CT in radiation therapy using planning MDCT images. *Med Phys*. 2010;37:5395-5406.
21. Park Y-K, Sharp GC, Phillips J, Winey BA. Proton dose calculation on scatter-corrected CBCT image: feasibility study for adaptive proton therapy. *Med Phys*. 2015;42:4449-4459.
22. Hofmaier J, Haehnle J, Kurz C, et al. Multi-criterial patient positioning based on dose recalculation on scatter-corrected CBCT images. *Radiother Oncol*. 2017;125:464-469.
23. Neppl S, Kurz C, Köpl D, et al. Measurement-based range evaluation for quality assurance of CBCT-based dose calculations in adaptive proton therapy. *Med Phys*. 2021;48:4148-4159.
24. Schmitz H, Rabe M, Janssens G, et al. Validation of proton dose calculation on scatter corrected 4D cone beam computed tomography using a porcine lung phantom. *Phys Med Biol*. 2021;66:175022.
25. Niepel K, Kamp F, Kurz C, et al. Feasibility of 4DCBCT-based proton dose calculation: an ex vivo porcine lung phantom study. *Z Med Phys*. 2019;29:249-261.
26. Bondesson D, Meijers A, Janssens G, et al. Anthropomorphic lung phantom based validation of in-room proton therapy 4D-CBCT image correction for dose calculation. *Z Med Phys*. 2022;32:74-84.
27. Feldkamp LA, Davis LC, Kress JW. Practical cone-beam algorithm. *J Opt Soc Am A*. 1984;1:612-619.
28. Mory C, Janssens G, Rit S. Motion-aware temporal regularization for improved 4D cone-beam computed tomography. *Phys Med Biol*. 2016;61:6856-6877.
29. Wolthaus JWH, Sonke J-J, van Herk M, Damen EMF. Reconstruction of a time-averaged midposition CT scan for radiotherapy planning of lung cancer patients using deformable registration. *Med Phys*. 2008;35:3998-4011.
30. Zijp L, Sonke J-J, van Herk M. Extraction of the respiratory signal from sequential thorax cone-beam X-ray images. In: 2004 International Conference on the Use of Computers in Radiation Therapy. 2004:507-509.
31. Rit S, Oliva MV, Brousmiche S, Labarbe R, Sarrut D, Sharp GC. The Reconstruction Toolkit (RTK), an open-source cone-beam CT reconstruction toolkit based on the Insight Toolkit (ITK). *J Phys Conf Ser*. 2014;489:012079.
32. Janssens G, Jacques L, de Xivry JO, Geets X, Macq B. Diffeomorphic registration of images with variable contrast enhancement. *Int J Biomed Imaging*. 2011;2011:1-16.
33. Meijers A, Knopf A-C, Crijns AP, et al. Evaluation of interplay and organ motion effects by means of 4D dose reconstruction and accumulation. *Radiother Oncol*. 2020;150:268-274.
34. Ribeiro CO, Visser S, Korevaar EW, et al. Towards the clinical implementation of intensity-modulated proton therapy for thoracic indications with moderate motion: robust optimised plan evaluation by means of patient and machine specific information. *Radiother Oncol*. 2021;157:210-218.
35. Paganetti H, Niemierko A, Ancukiewicz M, et al. Relative biological effectiveness (RBE) values for proton beam therapy. *Int J Radiat Oncol Biol Phys*. 2002;53:407-421.
36. Fredriksson A, Forsgren A, Hårdemark B. Minimax optimization for handling range and setup uncertainties in proton therapy. *Med Phys*. 2011;38:1672-1684.
37. Fox J, Ford E, Redmond K, Zhou J, Wong J, Song DY. quantification of tumor volume changes during radiotherapy for non-small-cell lung cancer. *Int J Radiat Oncol Biol Phys*. 2009;74:341-348.
38. Wolthaus JW, Sonke J-J, van Herk M, et al. Comparison of different strategies to use four-dimensional computed tomography in treatment planning for lung cancer patients. *Int J Radiat Oncol Biol Phys*. 2008;70:1229-1238.
39. Thing RS, Bernchou U, Hansen O, Brink C. Accuracy of dose calculation based on artefact corrected Cone Beam CT images of lung cancer patients. *Phys Imaging Radiat Oncol*. 2017;1:6-11.
40. Dong G, Zhang C, Deng L, et al. A deep unsupervised learning framework for the 4D CBCT artifact correction. *Phys Med Biol*. 2022;67:055012.
41. Hansen DC, Landry G, Kamp F, ei al. ScatterNet: a convolutional neural network for cone-beam CT intensity correction. *Med Phys*. 2018;45:4916-4926.
42. Landry G, Hansen D, Kamp F, et al. Comparing Unet training with three different datasets to correct CBCT images for prostate radiotherapy dose calculations. *Phys Med Biol*. 2019;64:035011.

**How to cite this article:** Schmitz H, Rabe M, Janssens G, et al. Scatter correction of 4D cone beam computed tomography to detect dosimetric effects due to anatomical changes in proton therapy for lung cancer. *Med Phys*. 2023;1-12. https://doi.org/10.1002/mp.16335

## APPENDIX

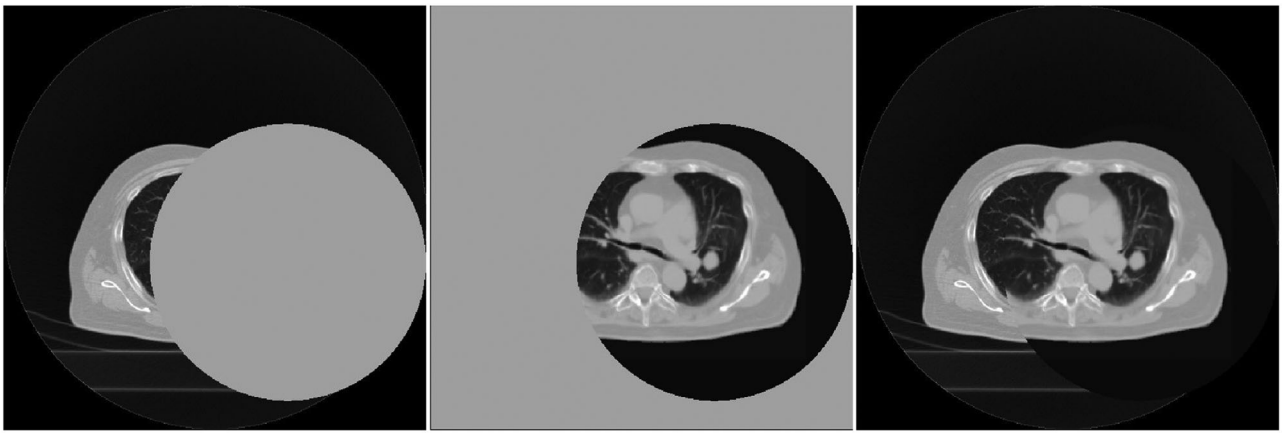

**FIGURE A.1** Steps of the stitching process of a single breathing phase for patient 14. Left: CT, which has all values inside the CBCT FOV set to zero. Middle: vCT, which has all values outside the CBCT FOV set to zero. Right: The addition of both modified CT and vCT, which is called stitched vCT. Within the scatter correction workflow, there is a couch removal step. Consequently, the initial CBCT, the vCT, and the $CBCT_{cor}$ do not show the couch. CBCT, cone beam computed tomography; FOV, field of view; vCT, virtual CT.

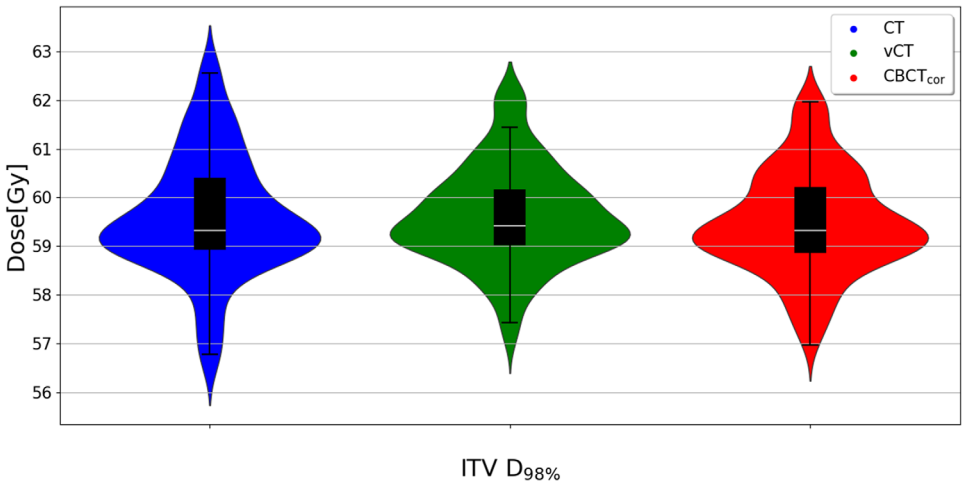


**FIGURE A.2** Violin plot showing the absolute dose of all 21 patients for ITV $D_{98\%}$ for all phases of CT, vCT, and $CBCT_{cor}$. Additionally, box plots with the median value shown as a white horizontal line and a whisker length of 1.5 times the interquartile range (25th to 75th percentile) are displayed. CBCT, cone beam computed tomography; ITV, internal target volume; vCT, virtual CT.